AIAA Aviation
16-20 June 2014, Atlanta, GA
32nd AIAA Applied Aerodynamics Conference

Numerical Analysis of Unsteady Aerodynamics of Formula Car during Dynamic Cornering Motion

Kohei Nara, Makoto Tsubokura, Jun Ikeda, and Urban Fasel
Hokkaido University, Faculty of Engineering, Kita 13, Nishi 8, Kita-ku, Sapporo, Hokkaido, 060-8628, Japan

Toyokazu Takemoto
Team Le Mans, 1157-340 Hotozawa, Gotenba, Shizuoka, 412-0046, Japan

Takuji Nakashima
Hiroshima University, Graduate School of Engineering 1-4-1, Kagamiyama , Higashi-Hiroshima, Hiroshima, 739-8527, Japan

Yoshihiro Sasaki
Numerical Flow Designing, 1-10-7-10F Higashi-Gotanda, Shinagawa-ku Tokyo, 141-0022, Japan

Aerodynamics is one of the most important elements when using formula-type vehicles in motorsport. Traditionally, estimating aerodynamic performance is mainly evaluated using a wind tunnel and steady-state simulation with a stationary vehicle. However, it is impossible to reproduce and estimate the flow field during cornering. For this reason, conducting aerodynamic simulation whilst considering the vehicle's motion can be effective.

The unsteady aerodynamic forces acting on a formula car, including the vehicle's motion, were investigated using large eddy simulation. The study was based on a simplified formula car model. Two moving boundary methods, Arbitrary Lagrangian-Eulerian (ALE) method and non-inertial frame of reference method, were applied to the cornering simulation. To represent the change in aerodynamic forces around a formula car in its cornering motion, aerodynamic forces in quasi-steady simulations and that during cornering were compared. Finally, the effect of slip, yaw motion, and acceleration against the aerodynamic forces and center of pressure was investigated.

Nomenclature

A_S	=	frontal projected area of the vehicle [m^2]
C_p	=	pressure coefficient
C_X	=	force coefficient in the x direction
C_Y	=	force coefficient in the y direction
C_Z	=	force coefficient in the z direction
C_S	=	Smagorinsky's constant
dt	=	time step
f_s	=	Van-Driest function
F_X	=	drag force [N]
F_Y	=	side force [N]
F_Z	=	lift force [N]
H	=	height of the vehicle [m]
L	=	length of the vehicle [m]
M_X	=	rolling moment[Nm]
M_Y	=	pitching moment[Nm]
M_Z	=	yawing moment[Nm]
p	=	static pressure of fluid
S_{ij}	=	strain rate tensor
t	=	time [sec.]
u_i	=	velocity for i direction [m/s]
W	=	width of the vehicle [m]

X, Y = absolute coordinate fixed on the ground
x, y = relative coordinate fixed on the vehicle
x_i = three components of the spatial coordinate
β = slip angle [deg]
θ = pitch angle [deg]
ν = kinetic viscosity [m^2/s]
ρ = density of the incoming fluid [kg/m^3]
φ = roll angle [deg]
ψ = yaw angle [deg]

I. Introduction

Speed and performance are critical in motorsport. When using formula-type race cars in particular, aerodynamics is one of the most important design considerations because properties, such as drag and lift coefficients, can have a profound effect on vehicle performance. In fact, Katz[1] suggested the more aerodynamic down force, the faster the speed during cornering. When a vehicle is running on a race circuit, there is a possibility that unsteady aerodynamic forces can appear due to rapid acceleration, deceleration, and changing in position. Traditionally, aerodynamic performance is mainly done through wind tunnel experiments and steady state simulation with a stationary vehicle using Reynolds averaged Navier-Stokes simulation (RANS). These methods can predict aerodynamic performance whilst running in a straight line, but it is difficult to duplicate and estimate the flow field during cornering.

On the other hand, the development of computational fluid dynamics (CFD) and high-performance supercomputers enables the operation of huge and sensitive aerodynamic simulations. For example, Watanabe et al.[2] reported the simulation of a high-speed vehicle negotiating a hairpin curve by using RANS and the Moving Computational Domain (MCD) method. Tsubokura et al.[3] also estimated aerodynamic performance of a vehicle in yawing motion by using large-eddy simulation (LES) and moving boundary methods. For all these reasons, unsteady CFD regarding a vehicle's dynamic motion is effective for estimating aerodynamic performance of a vehicle in motion and in an unsteady state.

When considering the method of simulating a vehicle negotiating a corner with CFD, two types of approaches can be considered. One is the non-inertial frame of reference method. However, if a cornering simulation were to be conducted with this method, instability of calculation would occur due to the governing equations becoming complex because of extra terms for apparent forces, such as the Coliolis force. The other approach is computing the vehicle's motion in a sub-grid. The sub-grid, including the vehicle, can move only inside the prepared main-grid. Therefore, in this study, two moving boundary methods were combined to represent the vehicle's dynamic motion in a numerical simulation.

The final goal with this research is to develop an aerodynamic evaluation method by simulating the cornering of a formula car and determining the unsteady aerodynamic characteristics in a vehicle's motion and flow mechanism. The objective with this study was to establish how to simulate a vehicle's motion and investigate the unsteady aerodynamic forces of a formula car during cornering, accelerating, and decelerating rapidly as a first step. The LES was used as the unsteady numerical analysis method. A vehicle's yaw and translational motions were reproduced using two moving boundary methods: the Arbitrary Lagrangian-Eulerian (ALE) method for the rotational motions and the Navier-Stokes equations in a non-inertial frame reference method for the translational motion. The vehicle's motion was applied by calculating and modeling driving test data.

II. Numerical Methods

A. Governing Equations

The governing equations used in this study are spatially filtered continuity and momentum equations for incompressible Newtonian flows.

$$\frac{\partial \bar{u}_i}{\partial x_i} = 0, \tag{1}$$

$$\frac{\partial \bar{u}_i}{\partial t} + \frac{\partial}{\partial x_j}\bar{u}_i\bar{u}_j = -\frac{\partial \bar{P}}{\partial x_i} + 2\frac{\partial}{\partial x_j}(\nu + \nu_{SGS})\bar{S}_{ij}, \tag{2}$$

where the over-bar indicates the spatially filtering operation for LES, and u_i, P, and ν are the velocity

components for the *i* direction, pressure, and kinetic viscosity, respectively. The strain rate tensor $\bar{S}_{ij}$ and the filtered pressure $\bar{P}$ in Eq. (2) are defined as

$$\bar{S}_{ij} = \frac{1}{2}\left(\frac{\partial \bar{u}_j}{\partial x_i} + \frac{\partial \bar{u}_i}{\partial x_j}\right). \quad (3)$$

$$\bar{P} = \frac{\bar{p}}{\rho} + \frac{1}{3}\left(\overline{u_k u_k} - \bar{u}_k \bar{u}_k\right), \quad (4)$$

where ρ is the density of the fluid. The subgrid-scale (SGS) eddy viscosity ν_{SGS} in Eq. (2) was modeled by Smagorinsky as

$$\nu_{SGS} = (C_s f_s \Delta)^2 \sqrt{\bar{S}_{ij}\bar{S}_{ij}}, \quad (5)$$

where C_s is the model coefficient and is given as 0.15[4]. The SGS turbulence length scale Δ is defined as the cube-root of the volume at each numerical element. To express the asymptotic behavior of the SGS eddy viscosity near the wall, a wall damping function, of van-Driest, f_s is multiplied with the SGS length:

$$f_s = 1 - exp\frac{-y^+}{25}, \quad (6)$$

where y^+ is the distance from the wall normalized by the surface friction and kinetic viscosity.

B. Discretization

The governing equations were discretized in space by using the vertex-centered unstructured finite volume method. The second-order central difference method was used to compute the spatial derivative. For the convective term in the momentum equation, the third-order upwind scheme was used. The time increment was based on the fractional step method developed by Kim and Moin[5], in which the Euler implicit method is used for the velocity prediction step. The pressure-velocity coupling was modeled with the simplified marker and cell (SMAC) algorithm developed by Amsden and Harlow[6]. The incomplete Cholesky conjugate gradient (ICCG) method was used to solve the pressure Poisson equation.

C. Moving Boundary Method

Two moving boundary methods were used to represent the vehicle's dynamic motion in the numerical simulation. The ALE method[7] was used to represent the vehicle's rotational motion. The deformation of the surrounding mesh around the vehicle was calculated by solving a virtual spring-mass system on the grid. In this study, we divided the numerical region into two parts to avoid excessive mesh distortion. The region around the vehicle was used for the rolling and pitching motions. The region far from the vehicle was used to represent the vehicle's yawing motion.

The other moving boundary method uses the governing equations in the non-inertial frame of reference method. This method was used for the vehicle's translational motion. The coordinate origin was fixed at the vehicle's center of gravity and the vehicle's translational acceleration was expressed in terms of the external forces in the momentum equations of the fluid. Yawing motion with the ALE method and translational motion with the non-inertial flame of reference method are shown in Figure 1. Cornering by combining the ALE and non-inertial frame of reference methods is shown in Figure 2.

The reason for using combined two methods is that the vehicle's translational motion has a relatively large

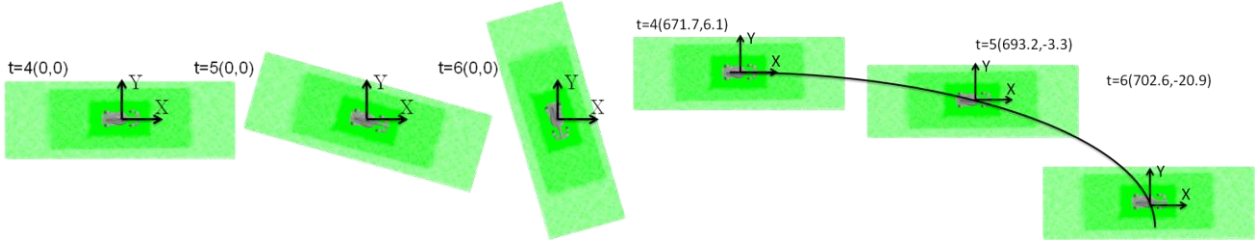

Figure 1. ALE method (left) and non-inertial frame of reference method (right)

displacement compared with its rotational motion, and this situation is difficult to treat with the ALE method.

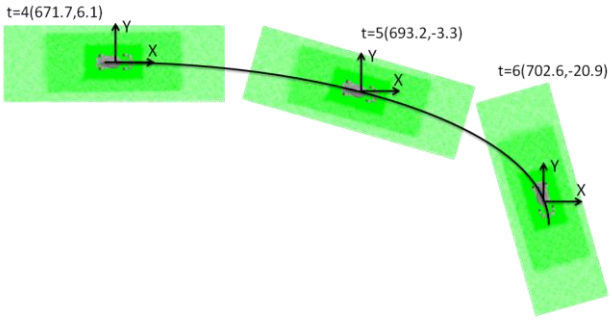

Figure 2. ALE and non-inertial frame of reference methods

D. Numerical Conditions

The analysis model and the definitions of aerodynamic forces and moments are shown in Figure 3. The model was based on the CAD data of a vehicle used by Super Formula "FN09". It was simplified by omitting the suspension, rough parts, and smoothing wheel shape. The length, width, and height of the model were L=4.80 m, W=2.00 m, and H=0.95 m, respectively. The computational domain, boundary conditions, and grid allocation on the ground are shown in Figure 4. The rectangular domain was L=5.38, W=7.5, and H=9.

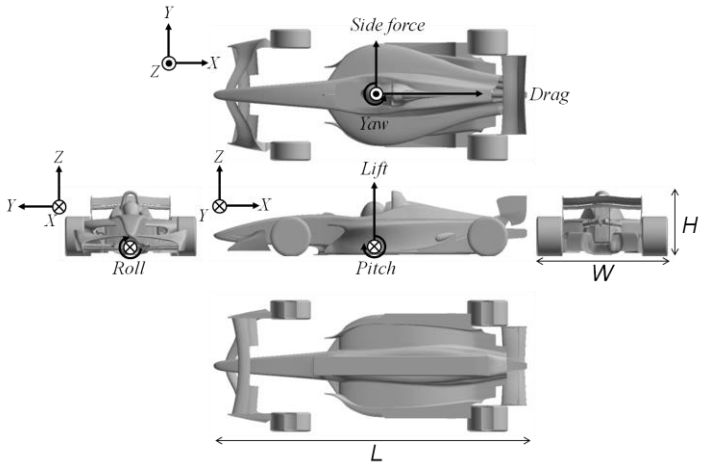

Figure 3. Target model (FN09); definition of forces and moments

The blockage ratio, calculated as the ratio of the project area of the vehicle to the flow passage area, is recommended not to be greater than 5% considering the effect of blockage against the steady aerodynamic force coefficient. By contrast, the blockage ratio of this study, 1.48%, is small enough to be discounted. Moreover, considering the effect of the slip angle of the vehicle, not only the blockage ratio of the main stream, but also that of the crosswind stream resulted in a smaller value, 0.65%.

As the boundary condition, the inlet velocity was set to be the same as the vehicle's velocity. In this case, the side wall was also set to an inlet condition to use the non-inertial frame of reference method. The top wall was set to a free slip condition, and the surface and floor of the vehicle were set to a log law boundary condition.

Figure 5 illustrates an unstructured grid on and around the vehicle. The surface resolution ranged from 1 to 15 mm. The entire numerical domain was filled in with tetrahedral elements. The total numbers of elements and nodes were about 46 million and 7.8 million, respectively.

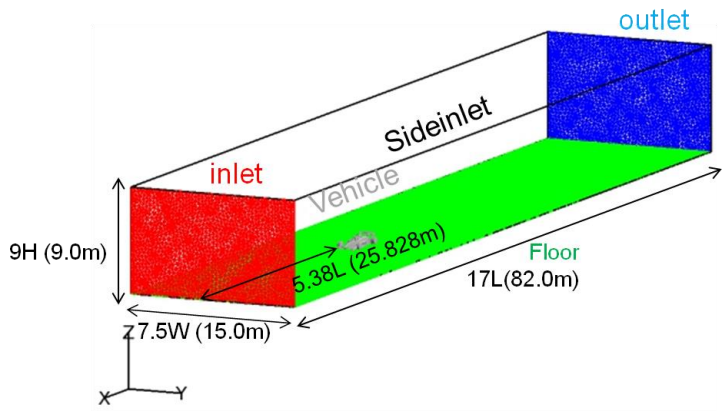

Figure 4. Computational domain and boundary conditions

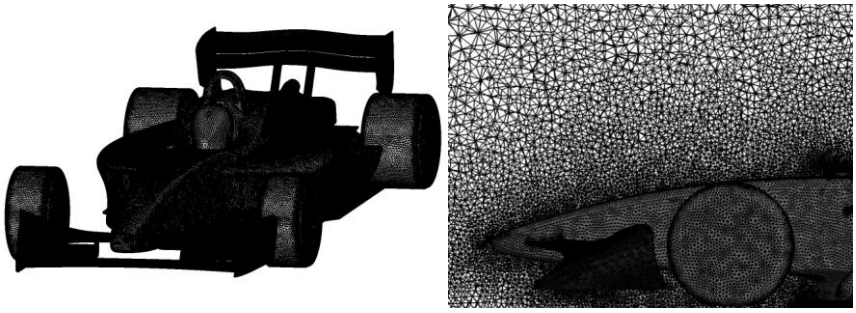

Figure 5. Grid resolution on vehicle body (left) and near-wall (right)

E. Software and Hardware

In this study, the unstructured finite-volume computational code called "FrontFlow/red-Aero" was used for conducting LES. All numerical simulations were conducted on the HITACHI SR16000 supercomputer at the Information Technology Center of Hokkaido University. A total of 16 nodes/512 CPUs were used.

F. Motion condition

Three corners were simulated to investigate the effect of cornering motion on aerodynamic forces. Figure 6 shows the Fuji Speed Way circuit and the three corners in which the simulation was conducted, 1st corner, 100R, and Hairpin corner. The vehicle's motion condition was set based on the position change data from the driving test data obtained from an actual vehicle running on the Fuji Speed Way circuit. These data were applied by calculating the position of the center of the vehicle and yaw angle from the acceleration, gyro, load of each wheel, and slip angle data, which were obtained from sensors. These experimental data were approximated with a continuous function as the numerical condition to prevent excessive numerical oscillations in the entire computational domain. The modeled track is shown in Figure 7.

Figure 6. Simulated corners (Fuji Speed Way circuit)

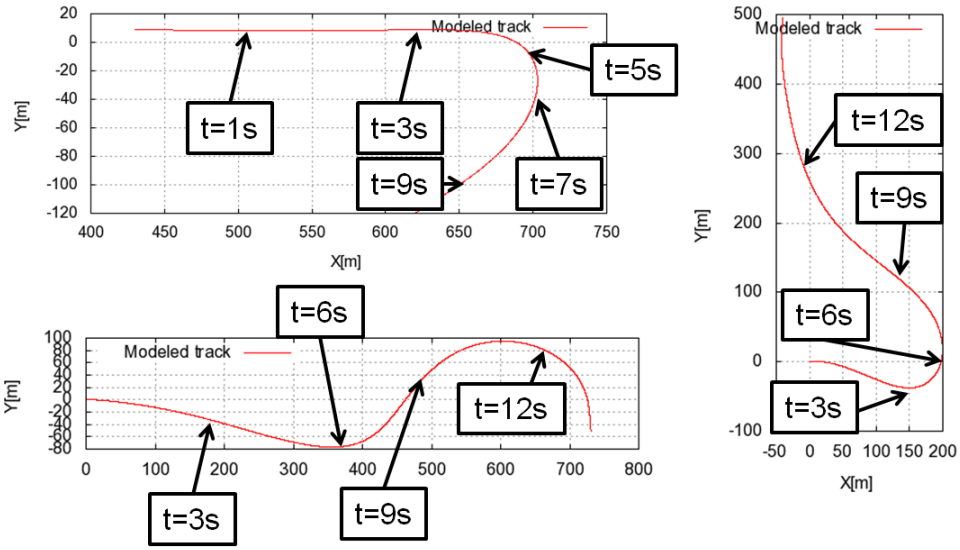

Figure 7. Modeled track (upper left: 1st corner, lower left: 100R, right: Hairpin corner)

G. Definition of the attitude angles

The vehicle was accompanied by translational motion and yaw rotational motion. The angle between the vehicle's central axis and X axis set in the analysis region is defined as the yaw angle ψ. There was always a gap between the tangential direction of the track of the vehicle's center and direction of the vehicle's central axis. This angle is defined as the slip angle β. Figure 8 shows the definitions of ψ and β. The basis of the yaw angle, coordinate system fixed at rest, is the vehicle's center at t=0. This axis is defined as the X axis.

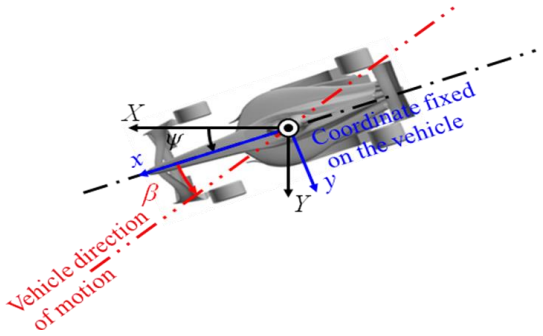

Figure 8. Definition of yaw angles and slip angle

III. Results and Discussions

A. Characteristics of corner and aerodynamic forces

Figure 9 shows the time series of surface pressure, velocity magnitude, iso-surface of velocity magnitude, and grid movement during cornering. We can confirm that the wake flow curves around the track of the vehicle's center.

Figures 10-12 show the time series of the aerodynamic coefficients of forces and moments and each corner. The vehicle's velocity and slip angle were set as a double axis. To represent the change in aerodynamic forces around a formula car in its cornering motion, aerodynamic forces in quasi-steady simulation and that of cornering were compared. Quasi-steady simulation was conducted with the vehicle's velocity and attitude angle maintained to predict the coefficient of the aerodynamic forces.

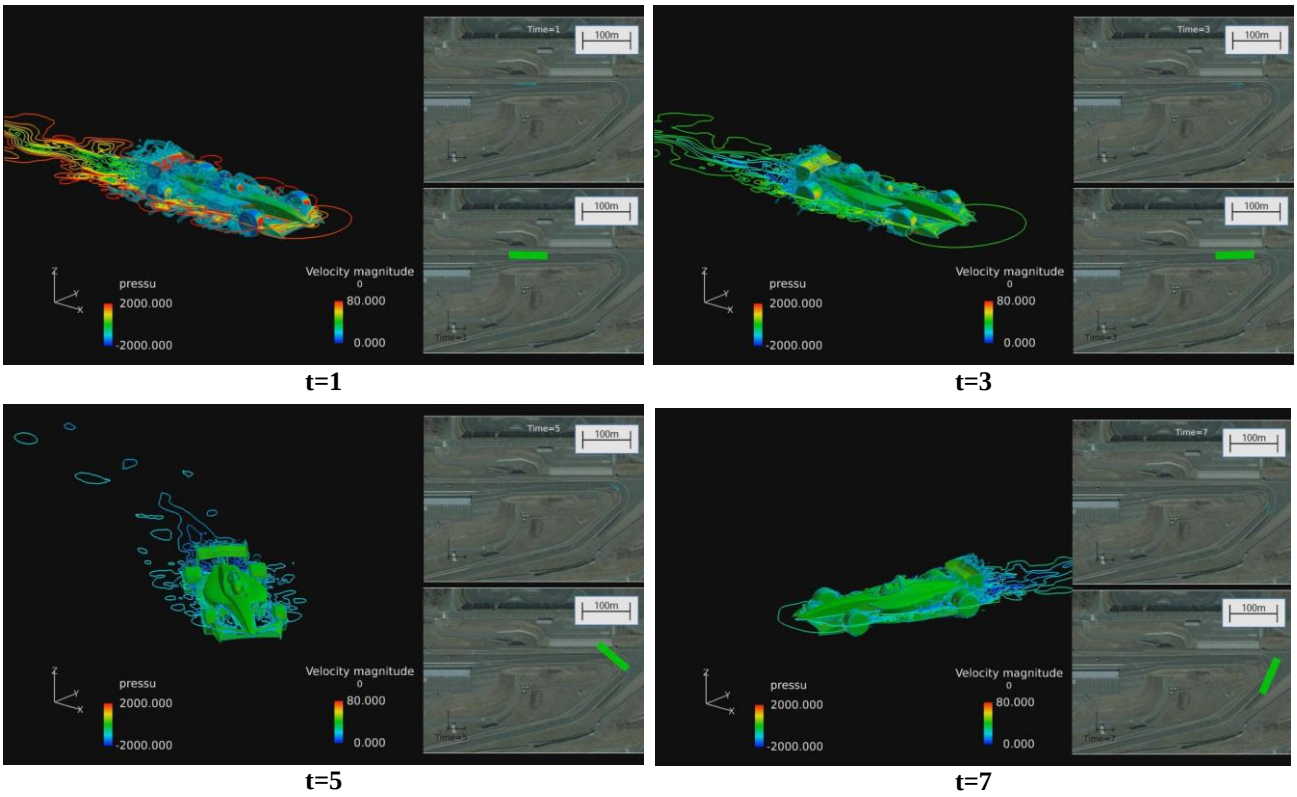

Figure 9. Flow field (left: surface pressure and velocity magnitude, upper right: iso-surface of velocity magnitude, lower right: computational domain)

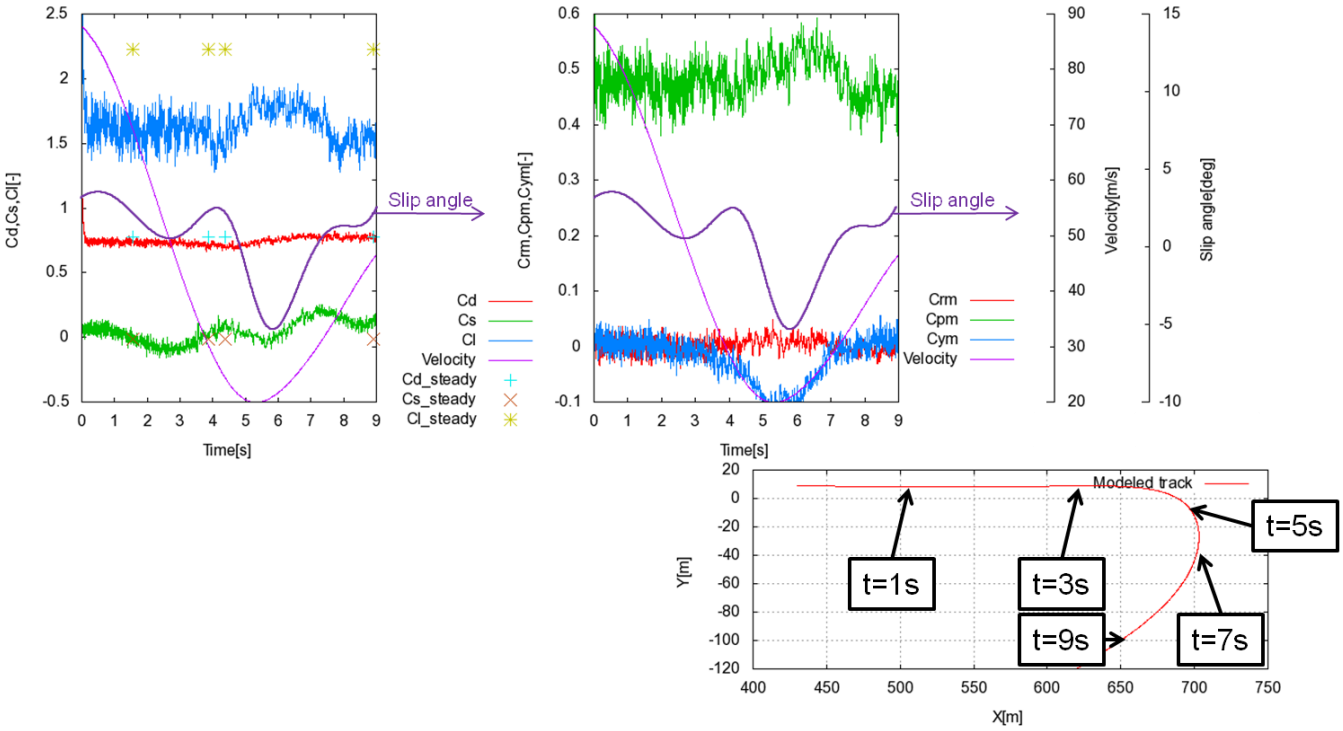

Figure 10. Time series of coefficients in 1st corner (left: forces, right: moments)

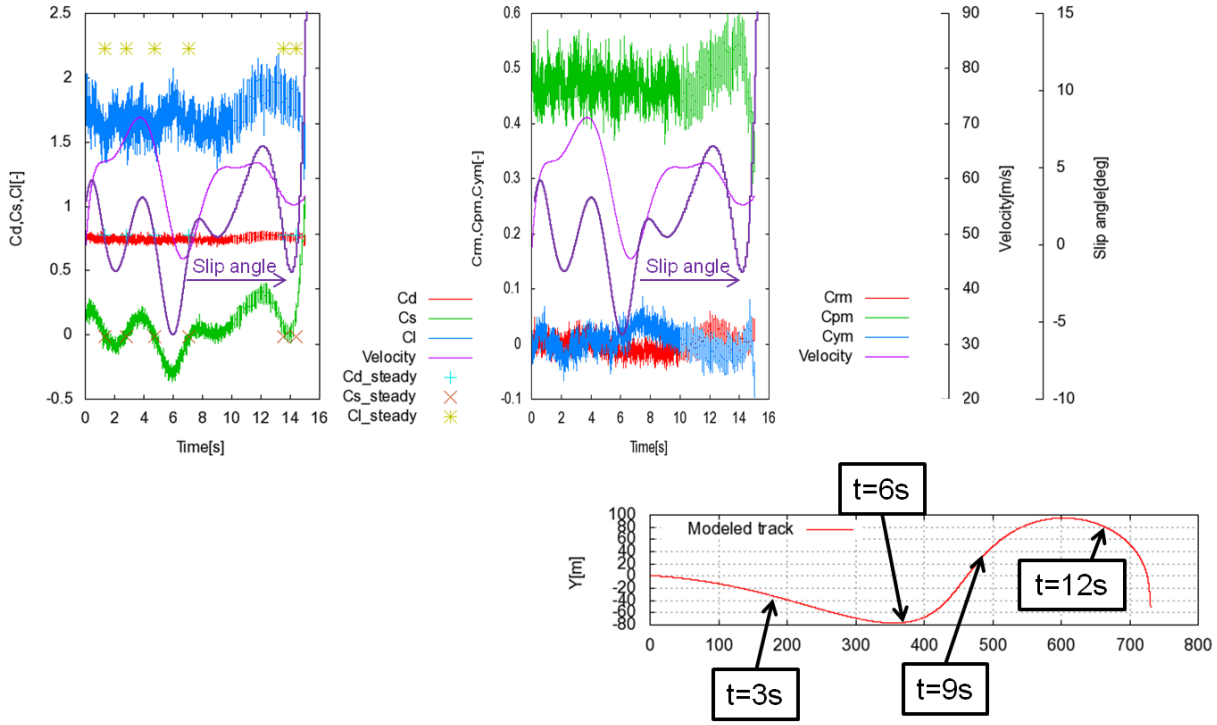

Figure 11. Time series of coefficients in 100R (left: forces, right: moments)

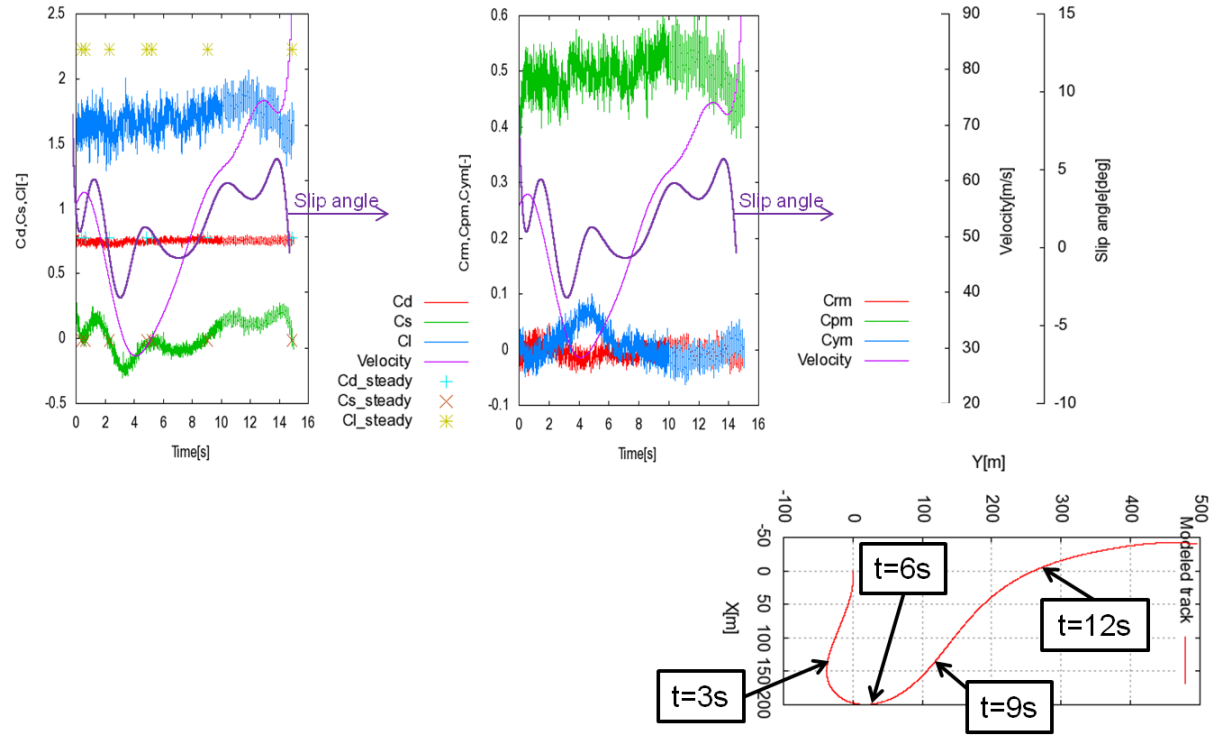

Figure 12. Time series of coefficients in Hairpin corner (left: forces, right: moments)

We first discuss the characteristics and aerodynamic coefficients of forces and moments for the 1st corner. A vehicle decelerated from 90 to 20 m/s in about 5 s. After deceleration, velocity increases from 20 to 50 m/s in about

four seconds. The vehicle began to slip at t=5 s, and slipped outward up to about 5 degrees at t=6 s near the outlet of the corner.
The side and down forces noticeably changed. The side force swayed due to the slip angle. the down force was larger between t=0 and 4 s in which the slip angle did not change much and the vehicle was in deceleration compared to that between t=7 and 9 s in which the slip angle did not change much, as between t=0 and 4 s, and the vehicle was in acceleration. On the other hand, there was a larger force between t=4 and 7 s, in which the slip angle changed more than that from t=0 to 4 s, and from t=7 to t=9 s, in which it did not change much.
The pitching and yawing moments noticeably changed. The yawing moment swayed due to the slip angle, as with the side force. The pitching moment was larger between t=0 and 4 s in which the slip angle did not change a much and the vehicle was in deceleration compared to that between t=7 and 9 s in which the slip angle did not change much, as between t=0 and 4 s, and the vehicle was in acceleration, as with the down force. On the other hand, there was a larger force between t=4 and 7 s in which the slip angle changed more than that from t=0 to 4 s and from t=7 to 9 s in which the slip angle did not change much.

We next discuss the characteristics and the aerodynamic coefficients of forces and moments regarding 100R. The vehicle accelerated by about 20 m/s in about 4 s and decelerated to 45 m/s between t=5 to 7 s. The vehicle accelerated to 60 m/s in 2 s and was constant for 4 s. After that, the vehicle began to decelerate. The vehicle began to slip at t=4 s, and slipped inward up to about 5 degrees at t=6 s near the outlet of the corner. After that, the vehicle began to slip at t=9 s, and slipped inward up to about 6 degrees at t=12 s near the outlet of the corner.
The side and down forces noticeably changed. The side force swayed due to the slip angle as well as those of the 1st corner. The down force swayed due to the absolute value of the slip angle from t=0 to 4 s in which the rate of change of the slip angle is large and the vehicle accelerated. The down force increased between t=4 to 6 s in which the vehicle did a large slide, and there was a larger force between t=4 and 6 s in which the slip angle changes quite a bit and the vehicle was in acceleration compared to that from t=7 to 9 s in which the slip angle did not change much and the vehicle was in acceleration. On the other hand, there was a larger force between t=4 and 7 s in which the slip angle changed quite a bit compared to that from t=7 to 9 s in which the slip angle did not change much. The down force decreased between t=7 and t=9 s, in which the vehicle's acceleration and the slip angle decreased, increased at t=12 when the vehicle slid, and decreased at t=14 s in which the vehicle was in gentle deceleration and the slip angle decreased.
The pitching and yawing moments noticeably changed as well in the 1st corner. The yawing moment swayed due to the slip angle, as the side force and that in the 1st corner. There was not such a large variation in the pitching moment in the first 10 s, though there were some fluctuations. However, it increased from t=10 to 12 s, in which the vehicle moved at a constant speed and the slip angle increased, and from t=12 to 14 s, in which the vehicle was in gentle deceleration and the slip angle decreased.

Finally, we discuss the characteristics and aerodynamic coefficients of forces and moments regarding the hairpin corner. The vehicle decelerated from 60 to 30 m/s in about 4 s. After that, it continued to accelerate until t=4 s. The vehicle slid inward up to about 5 degrees at t=1 s and slipped inward up to about 4 degrees at t=3. The vehicle swayed gently between t=4 and 8 s. It then slipped inward up to about 5 degrees at t=6 s near the outlet of the corner. After that, the vehicle began to slip at t=8 s, and slipped inward up to about 6 degrees at t=13.5 s near the outlet of the corner.
The side and down forces noticeably changed. The side force swayed due to the slip angle as in the other two corners. The down force swayed due to the absolute value of the slip angle from t=0 to 4 s in which the rate of change of the slip angle is large and the vehicle was in acceleration, as in 100R. The down force was approximately constant between t=4 and 8 s in which the rate of slipping did not increase much. On the other hand, The down force increased gently between t=8 and 12 s in which the slip angle increased and increased between t=12 and 14 s in which the vehicle was in gentle deceleration and was slipping.
The pitching and yawing moments noticeably changed, as in the 1st corner. The yawing moment swayed due to the velocity, unlike in the other two corners. The pitching moment swayed due to the absolute value of the slip angle from t=0 to 4 s in which the rate of change of the slip angle is large and the vehicle was in acceleration.

According to the aerodynamic coefficients of forces, we can confirm that the rise and fall of side force is dependent on the slip angle and that the rise and fall of the down force depends on the vehicle's velocity and slip angle.

B. Effect of acceleration in down force

There was a larger force between t=0 and 4 s in which the change in the slip angle did not change much and the vehicle was in deceleration compared to that between t=7 and 9 s in which the slip angle did not change much, as

between t=0 and 4 s, and the vehicle was in acceleration, as shown in Figure 10; 1st corner. In the comparison between the aerodynamic forces of the cornering simulation and that of the quasi-steady simulation, the forces in deceleration were larger than those in acceleration.

Figure 13 shows the surface pressure distribution under the vehicle during acceleration, deceleration, and constant velocity at no slip angle to investigate the relation between acceleration and aerodynamic forces. These figures were chosen from the simulation conducted at the 1st corner because the variation in the slip angle was the smallest of the three corners. These results illustrate that there is a large negative pressure region during deceleration, whereas there was hardly any region of negative pressure during acceleration. This is due to the hysteresis of velocity. Therefore, the velocity of flow under the vehicle act like the velocity of flow in last-minute.

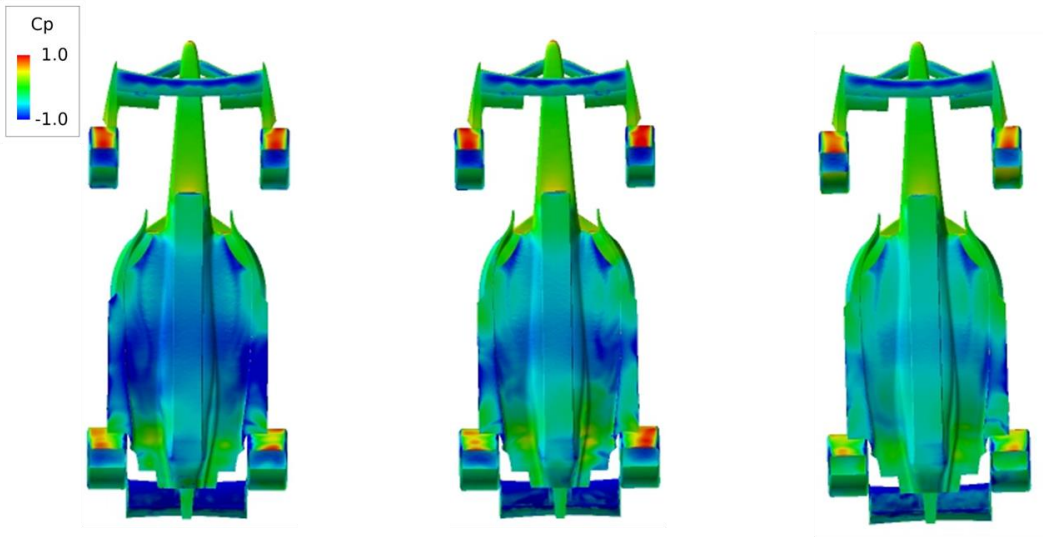

Figure 13. Surface pressure coefficient (left: deceleration, center: constant velocity, right: acceleration)

IV. Conclusion

We conducted LES for a formula car during acceleration, deceleration, and cornering by using the ALE and non-inertial frame of reference methods.

1. As a result of comparing the aerodynamic forces of the cornering simulation and that of the quasi-steady simulation, there were unsteady aerodynamic forces to vertical component in the vehicle's acceleration or sliding motion.
2. Moreover, a difference in unsteady aerodynamic forces may occur depending on not only the change in velocity but also that of acceleration and slip angle.

The above conclusions are a result of simulations that reproduced only translational motion and yaw rotational motion. Therefore, to estimate the aerodynamic characteristics of a vehicle, it is necessary to conduct a simulation not only for improving the approximation of the slip angle but also considering attitude variations, such as rolling and pitching motion.

Acknowledgments

This research was conducted collaboratively with Team Le Mans. This work was supported by the following grants: "Strategic Programs for Innovative Research" Field No. 4: Industrial Innovations from the Ministry of Education, Culture, Sports, Science, and Technology (MEXT)'s "Development and Use of Advanced, High-Performance, General-Purpose Supercomputers Project" and carried out in partnership with the University of Tokyo for the improvement of FrontFlow/red-Aero for High Performance Computing simulation; "Revolutionary Simulation Software (RSS21)" by MEXT for the development of FrontFlow/red; Industrial Technology Research Grant Program (2007-2011) from New Energy and Industrial Technology Development Organization (NEDO) for the development of simulation software "FrontFlow/red-Aero"; and Japan Society for the Promotion of Science (JSPS) Grant-in Aid for Scientific Research (KAKENHI) (B) Number 26289033 for the physical mechanism of

unsteady aerodynamics. Computational resources were provided with the following supercomputer systems: K computer at RIKEN AICS, HITACHI SR16000 M1 at Hokkaido University and FUJITSU FX10 at the University of Tokyo.

References

[1] Katz, J., Aerodynamics of Race Cars, Annual Reviews of Fluid Mechanics, Vol.38, (2006), pp.27-63.

[2] K.Watanabe,K.Matsuno,Moving ComputatinalDomain Method and Its Application to FlowAround aHifh-Speed Car Passing Through aHairpin Curve,Journal of computational Scienceand Technology, vol.3, No.2, (2009).

[3] Tsubokura, M., Yuki, I., Nakashima, T., Okada, Y., Kamioka, T., Nouzawa, T., "Unsteady Vehicle Aerodynamics during a Dynamic Steering Action: 2nd Report, Numerical Analysis", 2012, SAE Int. J. Passeng. Cars - Mech. Syst. May 2012 5:340-357.

[4] Smagorinsky, J.,"General Circulation Experiments with the Primitive Equations, I. The Basic Experiment", Monthly Weather Review, Vol.91(1963), pp.99-164.

[5] Kim, J., and Moin, P., 1985, "Application of a fractional-step method to incompressible Navier-Stokes equations" Journal of Computational Physics, 59, pp.308-323.

[6] Amsden, A. A., and Harlow, F. H., 1970, "A simplified MAC technique for incompressible fluid flow calculations", Journal of Computational Physics, 6, pp.322-325.

[7] Hirt C.W., Amsden A. A. andCook J.L.,"An arbitrary lagrangian–eulerian computingmethod for all flow speeds",Journal of Computational Physics, Vol. 14, No. 3 (1974), pp. 227-25.

[8] Hucho, W. H. and Sovran, G, "Aerodynamics of road vehicles", Annual Review of Fluid Mechanics, Vol. 25 (1993), pp.485-537.